Journal of Applied Physics

RESEARCH ARTICLE | MARCH 06 2025

Thermophysical property measurement of GaN/SiC, GaN/AlN, and AlN/SiC epitaxial wafers using multi-frequency/spot-size time-domain thermoreflectance

Husam Walwil ; Yiwen Song ; Daniel C. Shoemaker ; Kyuhwe Kang ; Timothy Mirabito ; Joan M. Redwing ; Sukwon Choi

J. Appl. Phys. 137, 095105 (2025)
https://doi.org/10.1063/5.0245381
CHORUS

Journal of Applied Physics ARTICLE pubs.aip.org/aip/jap

Thermophysical property measurement of GaN/SiC, GaN/AlN, and AlN/SiC epitaxial wafers using multi-frequency/spot-size time-domain thermoreflectance

Cite as: J. Appl. Phys. **137**, 095105 (2025); doi: 10.1063/5.0245381
Submitted: 25 October 2024 · Accepted: 8 February 2025 ·
Published Online: 6 March 2025

Husam Walwil,[1] Yiwen Song,[1] Daniel C. Shoemaker,[1] Kyuhwe Kang,[1] Timothy Mirabito,[2] Joan M. Redwing,[2] and Sukwon Choi[1,a)]

AFFILIATIONS

[1]Department of Mechanical Engineering, The Pennsylvania State University, University Park, Pennsylvania 16802, USA
[2]Department of Materials Science and Engineering, The Pennsylvania State University, University Park, Pennsylvania 16802, USA

[a)]**Author to whom correspondence should be addressed:** sukwon.choi@psu.edu

ABSTRACT

Gallium nitride (GaN)-based high electron mobility transistors (HEMTs) are essential components in modern radio frequency power amplifiers. In order to improve both the device electrical and thermal performance (e.g., higher current density operation and better heat dissipation), researchers are introducing AlN into the GaN HEMT structure. The knowledge of thermal properties of the constituent layers, substrates, and interfaces is crucial for designing and optimizing GaN HEMTs that incorporate AlN into the device structure as the barrier layer, buffer layer, and/or the substrate material. This study employs a multi-frequency/spot-size time-domain thermoreflectance approach to measure the anisotropic thermal conductivity of (i) AlN and GaN epitaxial films, (ii) AlN and SiC substrates, and (iii) the thermal boundary conductance for GaN/AlN, AlN/SiC, and GaN/SiC interfaces (as a function of temperature) by characterizing GaN-on-SiC, GaN-on-AlN, and AlN-on-SiC epitaxial wafers. The thermal conductivity of both AlN and GaN films exhibits an anisotropy ratio of ∼1.3, where the in-plane thermal conductivity of a ∼1.35 μm thick high quality GaN layer (∼223 W m^{-1} K^{-1}) is comparable to that of bulk GaN. A ∼1 μm thick AlN film grown by metalorganic chemical vapor deposition possesses a higher thermal conductivity than a thicker (∼1.4 μm) GaN film. The thermal boundary conductance values for a GaN/AlN interface (∼490 MW m^{-2} K^{-1}) and AlN/SiC interface (∼470 MW m^{-2} K^{-1}) are found to be higher than that of a GaN/SiC interface (∼305 MW m^{-2} K^{-1}). This work provides thermophysical property data that are essential for optimizing the thermal design of AlN-incorporated GaN HEMT devices.

I. INTRODUCTION

Gallium nitride (GaN) is particularly well-suited for the development of electronic devices that require high power and frequency operation, by taking advantage of the large bandgap energy (3.4 eV) and the critical breakdown field. Notably, GaN high electron mobility transistors (HEMTs) are ever-important components in the deployment of fifth-generation (5G) wireless communication systems and advanced radar systems in the form of radio frequency (RF) power amplifiers.[1–5] Unfortunately, commercial GaN HEMTs need to be operated under derated power conditions in order to reduce the channel temperature rise caused by undesirable self-heating effects.[6] Therefore, effective thermal management solutions are of paramount importance for GaN HEMTs to realize their full potential.

Silicon carbide (SiC) has been established as the primary substrate used for GaN power amplifiers. A schematic of a typical GaN-on-SiC HEMT is demonstrated in Fig. 1(a). The use of a SiC substrate offers many benefits such as high thermal conductivity,[7] relatively low lattice mismatch with GaN,[8] and semi-insulating characteristics.[9] Typically, a thin AlN nucleation layer is used to enable high quality heteroepitaxial growth of the GaN layer.[10]

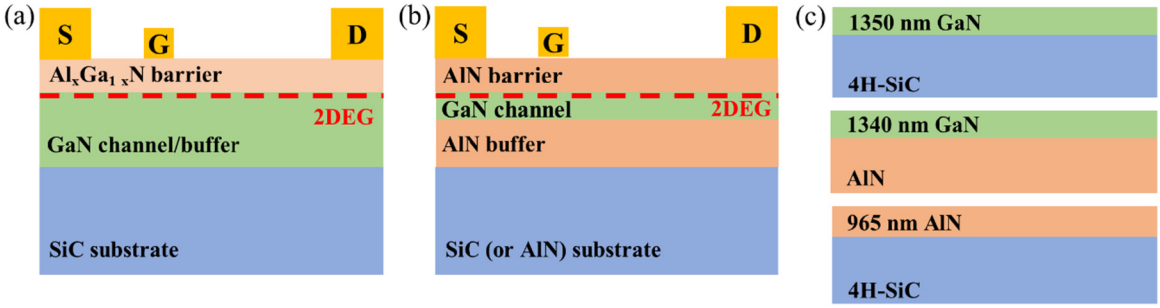

FIG. 1. Cross-sectional schematics of (a) an AlGaN/GaN HEMT grown on a SiC substrate and (b) an AlN/GaN/AlN HEMT fabricated on SiC or AlN substrates. (c) Cross-sectional schematics of the GaN-on-SiC, GaN-on-AlN, and AlN-on-SiC epitaxial wafers.

Recently, there has been a momentum on incorporating AlN into the GaN HEMT structure to achieve enhanced electrical performance, as shown in Fig. 1(b). For instance, this AlN/GaN/AlN platform employs a strained GaN quantum well sandwiched between AlN barrier and buffer layers, where the large bandgap energy difference results in effective electron confinement and the larger polarization discontinuity induces a higher two-dimensional electron gas (2DEG) density.[11,12] This has rendered AlN/GaN/AlN HEMT devices to exceed 24 W/mm power density operation at moderate drain-source voltage levels.[13] From a heat transfer point of view, AlN is known to possess a thermal conductivity that is comparable to that of SiC. However, the adoption of an AlN substrate may offer an added benefit of a reduced effective thermal boundary resistance (TBR) between the buffer layer and the substrate, which can lead to similar or better thermal performance compared to GaN-on-SiC devices.[14,15]

To a create a device thermal model that can evaluate the potential enhancement in the thermal performance of AlN-incorporated GaN HEMT structures, a complete knowledge of phonon transport within the epitaxial film and the substrate, and across the film/substrate interface is necessary. In other words, the anisotropic thermal conductivities of the epitaxial layers (GaN or AlN) and the substrate (SiC or AlN), as well as the thermal boundary resistance at the epitaxial layer/substrate interface must be measured as a function of temperature (i.e., over the operational temperature range). However, experimentally determining all the aforementioned thermophysical properties is challenging since it is difficult to simultaneously determine multiple unknown parameters from a single measurement. Most of previous studies on GaN epitaxial wafers have focused on characterizing the thermal conductivity of the epitaxial film, often lacking information on the anisotropy, which may lead to inaccurate determination of the interfacial thermal boundary resistance.[10,16–18] In addition, experimental data regarding the thermal boundary resistance associated with GaN/AlN and AlN/SiC interfaces are lacking in the literature.

In this study, GaN-on-AlN, GaN-on-SiC, and AlN-on-SiC epitaxial wafers were characterized using a multi-frequency/spot-size time-domain thermoreflectance (TDTR) approach to measure the anisotropic thermal conductivity of the epitaxial layers and substrates as a function of temperature. In addition, the thermal boundary resistance between the epitaxial layer and the substrate was characterized, also as a function of temperature.

II. SAMPLE DESCRIPTION

GaN-on-SiC, GaN-on-AlN, and AlN-on-SiC epitaxial wafers were characterized in this work, as illustrated in Fig. 1(c). The first GaN-on-SiC wafer shown in Fig. 1(c) (upper schematic) consists of a 1350 nm thick GaN film epitaxially grown on a 4H-SiC substrate using a ∼20 nm thick AlN interlayer, via metalorganic chemical vapor deposition (MOCVD). The GaN-on-AlN wafer illustrated in Fig. 1(c) (middle schematic) includes a 1340 nm thick GaN film directly grown on a 2″ single-crystal AlN substrate via MOCVD. The AlN-on-SiC wafer shown in Fig. 1(c) (lower schematic) includes an MOCVD-grown 965 nm thick AlN film deposited onto a 4H-SiC substrate. The thicknesses of the GaN and AlN films were determined via cross-sectional scanning electron microscopy (SEM) and spectroscopic ellipsometry.

III. MULTI-FREQUENCY/SPOT-SIZE TIME-DOMAIN THERMOREFLECTANCE

Time-domain thermoreflectance (TDTR) was used to measure the anisotropic thermal conductivities of the epitaxial films (GaN and AlN layers) and the substrates (4H-SiC and AlN), in both out-of-plane (κ_{out}; along the c-axis) and in-plane (κ_{in}; across the c-plane) directions. In addition, the thermal boundary conductance (*TBC*; inverse of the thermal boundary resistance, TBR) at the GaN/SiC, GaN/AlN, and AlN/SiC interfaces was characterized. Briefly, during TDTR measurements,[19] the sample is heated by a train of modulated ultrafast laser pulses (i.e., the pump laser beam at a frequency f, typically ranging from 0.1 to 20 MHz[20]), and the temperature response of the sample surface is detected by a time-delayed laser pulse (i.e., the probe beam) using a balanced photodetector and an RF lock-in amplifier. Objective lenses are used to concentrically focus both the pump and probe beams onto the sample surface and to control the laser spot size (w) ranging approximately from 4 to 40 μm ($1/e^2$ diameter). Details of the TDTR setup can be found in previous work.[21] To prepare the samples for TDTR measurements, an ∼80 nm thick aluminum (Al) transducer was deposited on the sample surface via RF sputtering.

The thickness of the Al film was determined by TDTR picosecond acoustics. The thermal conductivity of the Al film was determined based on the electrical resistivity measured by a four-point probe and using the Wiedemann–Franz law. TDTR measurements were first performed on bare 4H-SiC and AlN substrates (without epitaxial layers grown on them) to determine their anisotropic thermal conductivity values. After this, the epitaxial wafers including the MOCVD-grown films (GaN or AlN) were characterized to measure κ_{out}, κ_{in}, and the *TBC* between the epitaxial films and the substrate materials.

The sensitivity coefficient, $S_\alpha = \frac{\partial \ln R}{\partial \ln \alpha}$, reflects how responsive the measured TDTR ratio signal (R) is to a parameter α (e.g., κ_{out}, κ_{in}, or *TBC*).[19] Figure 2(a) displays the calculated sensitivity for a GaN-on-SiC wafer examined in previous studies, commonly utilizing $f = 3$ MHz and $w = 15\,\mu$m.[17,18,22] The calculations assumed $TBC_{GaN/SiC} \sim 250$ MW m^{-2} K^{-1} and $TBC_{Al/GaN} \sim 90$ MW m^{-2}K^{-1} as reported in these studies. The plot also illustrates the sensitivity to GaN films with thicknesses (h_{GaN}) of 500 and 1000 nm, when assuming isotropic thermal conductivities of 100 and 125 W m^{-1} K^{-1}, respectively.[17,18,22] In the calculations, a κ_{out} of 330 W m^{-1} K^{-1} for the SiC substrate was used. Volumetric heat capacities of 2.43, 2.65, and 2.13 MJ m^{-3} K^{-1} were used for the Al transducer, GaN films, and SiC substrate, respectively.

Figure 2(a) shows that the measurement sensitivity to the out-of-plane thermal conductivity of GaN ($\kappa_{out\text{-}GaN}$) and $TBC_{GaN/SiC}$ exhibits a similar trend/shape across the entire range of the delay time. This indicates that the data fitting results will influence each other. The low frequency (3 MHz) pump laser probes deep into the sample, thereby making the TDTR signal to be sensitive to both $\kappa_{out\text{-}GaN}$ and $TBC_{GaN/SiC}$. In Fig. 2(a), the average sensitivity ratio, $\frac{S_{TBC_{GaN/SiC}}}{S_{\kappa_{out-GaN}}}$, is ∼1.2. Therefore, a 10% error in the value of $\kappa_{out\text{-}GaN}$ would result in an 8% error in the value of $TBC_{GaN/SiC}$. Despite this, a common practice in previous studies[17,18,22] has been to simultaneously extract $\kappa_{out\text{-}GaN}$ and $TBC_{GaN/SiC}$, in addition to the *TBC* at the Al transducer/GaN interface ($TBC_{Al/GaN}$), ending up with inaccurate and/or non-unique combinations of $\kappa_{out\text{-}GaN}$ and $TBC_{GaN/SiC}$. Furthermore, while it is often assumed that the GaN film has isotropic thermal conductivity,[10,17,18] Fig. 2(a) shows that for a GaN film with thickness of $h_{GaN} = 1000$ nm, the sensitivity to the in-plane thermal conductivity of the GaN layer ($\kappa_{in\text{-}GaN}$) is not negligible. The sensitivity ratio, $\frac{S_{\kappa_{out-GaN}}}{S_{\kappa_{in-GaN}}}$, is ∼2, implying that a 20% error in $\kappa_{in\text{-}GaN}$ would result in a 10% error in $\kappa_{out\text{-}GaN}$. This is because when using a low frequency (3 MHz) pump laser, heat transfer does not occur in a purely one-dimensional regime.

In this regard, few attempts have been made to overcome the abovementioned challenges. One study attempted to reduce h_{GaN} in order to increase the measurement sensitivity to $TBC_{GaN/SiC}$ while decreasing the sensitivity to $\kappa_{out\text{-}GaN}$.[17] However, Fig. 2(a) shows that reducing h_{GaN} from 1000 to 500 nm increases the sensitivity to the thermal conductivity of the SiC substrate, without significantly altering the sensitivity to $\kappa_{out\text{-}GaN}$. More importantly, a reduction in h_{GaN} results in a decrease in the sensitivity to $TBC_{GaN/SiC}$. Another report attempted to perform measurements on multiple samples with varying h_{GaN} while assuming a thickness-independent GaN thermal conductivity to derive $TBC_{GaN/SiC}$.[22] However, an inaccurate estimation of this thickness dependence[23] and the high sensitivity to $\kappa_{out\text{-}GaN}$ may lead to unreliable results.

Therefore, in this work, a multi-frequency/spot-size TDTR approach was developed to selectively manipulate the TDTR measurement sensitivity so that each thermophysical property under interest could be accurately determined. It should be noted that the

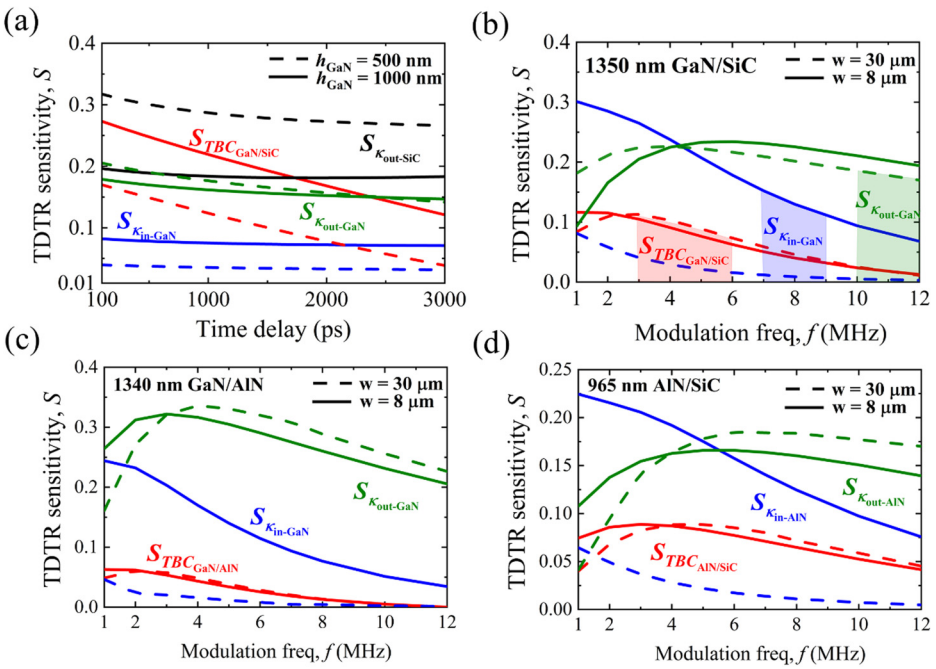

FIG. 2. (a) The calculated sensitivity of the TDTR ratio signal for an exemplar GaN-on-SiC material stack plotted as a function of pump-probe delay time for GaN film thicknesses (h) of 500 and 1000 nm. Calculations were performed using a single frequency of 3 MHz and a single spot diameter of 15 μm. The thermal conductivity of the GaN layer and the GaN/SiC *TBC* were taken from references.[17,18,22] The calculated sensitivity of the TDTR ratio signal for the (b) GaN-on-SiC, (c) GaN-on-AlN, and (d) AlN-on-SiC epitaxial wafers plotted as a function of modulation frequency (f) and spot sizes (w) of 8 and 30 μm. Calculations were performed for a delay time of 1000 ps.

multi-frequency/spot-size TDTR approach has been previously demonstrated to measure the heat capacity of films[24] and the anisotropy of bulk samples,[25] and to analyze the phonon mean free path (MFP).[26,27] Figure 2(b) shows a sensitivity plot for the GaN-on-SiC epitaxial wafer depicted in Fig. 1(c) (upper schematic). The sensitivity calculations are based on the anisotropic thermal conductivities of GaN and SiC as well as $TBC_{\mathrm{GaN/SiC}}$ at 300 K (each value can be found in Figs. 3, 4, and 7, respectively). For $f = 10$ MHz and $w = 30\,\mu$m, the sensitivity ratios $\frac{S_{\kappa_{\text{out-GaN}}}}{S_{\kappa_{\text{in-GaN}}}}$ and $\frac{S_{TBC_{\mathrm{GaN/SiC}}}}{S_{\kappa_{\text{out-GaN}}}}$ are 20 and 10, respectively, suggesting that $\kappa_{\text{out-GaN}}$ can be independently determined without any prior knowledge of $\kappa_{\text{in-GaN}}$ and $TBC_{\mathrm{GaN/SiC}}$. Furthermore, while the sensitivity to $TBC_{\mathrm{GaN/SiC}}$ remains unaffected by the spot size, $\kappa_{\text{in-GaN}}$ is significantly influenced by it. This allows to separately measure $TBC_{\mathrm{GaN/SiC}}$ and $\kappa_{\text{in-GaN}}$. For instance, the sensitivity ratio $\frac{S_{TBC_{\mathrm{GaN/SiC}}}}{S_{\kappa_{\text{in-GaN}}}}$ at $f = 5$ MHz and $w = 30\,\mu$m is approximately 4.5, implying that an error of 20% in $\kappa_{\text{in-GaN}}$ would result in only a 4.0% error in $TBC_{\mathrm{GaN/SiC}}$.

Measurements of the three epitaxial wafers were conducted across a pump modulation frequency range of 1–12 MHz for two spot sizes ($1/e^2$ diameter) of 8 and 30 μm. Values for κ_{out}, κ_{in} of the epitaxial film (i.e., GaN or AlN) and the *TBC* between the film and substrate (i.e., SiC or AlN) were determined by fitting the ratio of the in-phase and out-of-phase signals ($V_{\text{in}}/V_{\text{out}}$) from the RF lock-in amplifier to the solution of the heat diffusion equation for a multi-layer material stack.[28] After this, an iterative fitting process was performed until a single set of the three parameters (i.e., κ_{out}, κ_{in}, and *TBC*) would match all the measurement data. The uncertainties associated with the TDTR fitted parameters were estimated by considering the sensitivity of the TDTR ratio signal to the input parameters for the thermal model and their uncertainties: laser spot size (4%), κ_{Al} (5%), volumetric heat capacities (4%), *TBC* at the Al/epitaxial layer (i.e., GaN or AlN) and Al/substrate (i.e., SiC or AlN) interfaces (10%), and thickness of each layer (3% for Al and 5% for the epitaxial layer). In addition, the sensitivity of the TDTR signal to the absolute value of the phase and the uncertainty associated with determining the phase were accounted for. More details can be found in Ref. 29. Since the κ_{out} of the epitaxial layer is measured using a frequency and spot size of, for instance, 10 MHz and 30 μm, respectively, uncertainty contributions from the κ_{in} of the epitaxial layer and the *TBC* across the epitaxial layer/substrate interface are negligible. Similarly, since the TBC across epitaxial layer/substrate is measured using a frequency and spot size of, for example, 5 MHz and 30 μm, respectively, the uncertainty contribution from the κ_{in} of the epitaxial layer is minimal, while error propagation associated with the uncertainty in the κ_{out} of the epitaxial layer must be accounted for. Regarding the uncertainty in the κ_{in} of the epitaxial layer, error propagation associated with both uncertainties in the κ_{out} of the epitaxial layer and the TBC across epitaxial layer/substrate interface was included in the uncertainty calculation process. Temperature-dependent heat capacity values were adopted from the literature.[30]

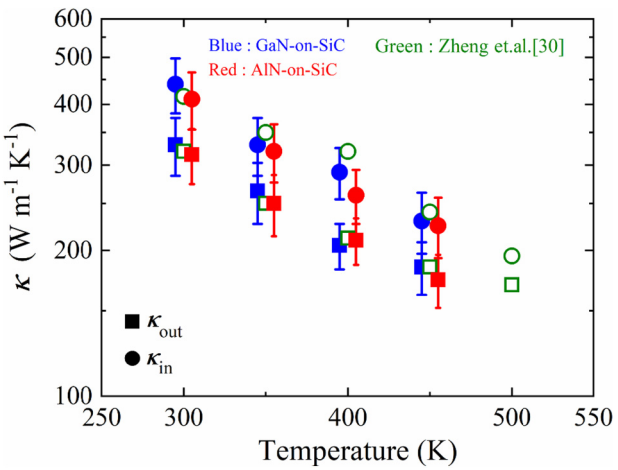

FIG. 3. The measured κ_{out} (squares) and κ_{in} (circles) of the 4H-SiC substrates as a function of temperature. For better visibility, the blue and red data points were, respectively, shifted to the left and right by 5 K.

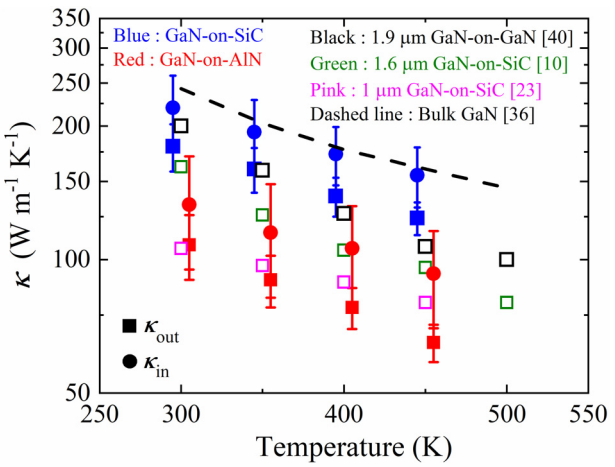

FIG. 4. The measured κ_{out} (squares) and κ_{in} (circles) for the GaN films grown on 4H-SiC (blue) and AlN (red). Open symbols represent the literature values for a 1.9 μm thick GaN film grown on GaN (black), 1.6 μm GaN film grown on SiC (green), and a 1 μm GaN film on SiC (pink). The dashed line represents the calculated thermal conductivity of bulk GaN by Lindsay *et al.*[36] For better visibility, the blue and red data points were, respectively, shifted to the left and right by 5 K.

The κ_{out} and κ_{in} of bare AlN and 4H-SiC substrates (with no GaN or AlN layer grown on them) were determined prior to performing TDTR measurements on the three epitaxial wafers shown in Fig. 1(c). It should be noted that, for a spot-size greater than 15 μm in diameter, no dependence on the spot size or frequency was observed when measuring both the κ_{out} and κ_{in} of the SiC or AlN substrates. On the other hand, when measuring the κ_{in} of the GaN and AlN epitaxial films, no variations were observed for measurements taken using 8 and 15 μm spot sizes. These observations are in agreement with those reported in previous studies.[30–32]

IV. MATERIAL CHARACTERIZATION

X-ray diffraction (XRD) was used to assess the crystalline quality of the GaN films grown on the SiC and AlN substrates.

High-resolution 2θ-ω, ω, ϕ, and chi scans were collected using a Malvern PANalytical Materials Research Diffractometer (MRD) system in the line focus mode using Cu $K_{\alpha 1}$ radiation. The detector (PIXcel 3D with 10 mm beam mask and ¼ degree divergence slit) was aligned to the (002) GaN film peak at approximately 34.625° 2θ. Rocking curves were collected over a range of 0.500° with a step size of 0.001° and a dwell time of 0.100 s. The full width at half maximum (FWHM) was extracted for each rocking curve to calculate the dislocation densities. Screw type dislocations were calculated using rocking curves collected for the (002) plane, while the edge-type dislocations were based on rocking curves collected for the (102) planes.[33,34]

Room temperature Raman spectra were collected as an additional method to qualitatively assess the crystalline quality of the GaN films. A Horiba LabRAM HR Evolution Raman microscope with a 532 nm excitation laser and 1800 groove/mm grating was used to monitor the E_2 (high) phonon mode of GaN. According to the energy-time uncertainty principle, the measured phonon linewidth broadens for lower crystalline quality films because of the reduced phonon lifetime. In addition, film residual stress was determined using Raman spectroscopy, based on the peak position of the E_2(high) phonon mode of GaN. Details of the stress measurement and calculation processes have been demonstrated by Choi *et al.*[35]

V. RESULTS AND DISCUSSION

Figure 3 shows the measured out-of-plane (κ_{out}; along the c-axis) and in-plane (κ_{in}; across the c-plane) thermal conductivities of the 4H-SiC substrates (of the GaN-on-SiC and AlN-on-SiC wafers) as a function of temperature. Both 4H-SiC substrates display similar values, with an anisotropy ratio of ~1.3. These findings are consistent with values reported in the literature, as shown in Fig. 3.[30]

The κ_{out} and κ_{in} of the GaN films are plotted in Fig. 4. The GaN grown on the AlN substrate exhibits a lower thermal conductivity compared to GaN grown on 4H-SiC. This discrepancy is attributed to the higher dislocation density in the GaN film grown on AlN as shown in Table I, due to the lack of an optimized interlayer compared to the GaN-on-SiC sample. The lattice mismatch is quite large between GaN and both AlN (~2.57%) and SiC (~3.57%). It should be noted that the thin AlN interlayer introduced into the GaN-on-SiC epitaxial wafer was used to mitigate the mismatch between GaN and 4H-SiC. The interlayer growth conditions (thickness, growth temperature, etc.) were optimized to give the best crystal quality in the GaN film. The interlayer possesses dislocations; therefore, it reduces the epitaxial mismatch stress such that the GaN layer can grow more in a 2D rather than 3D mode.

The edge and screw dislocation densities in the GaN films grown on 4H-SiC and AlN were calculated from the XRD rocking curves shown in Figs. 5(a) and 5(b) for the (102) and (002) reflections of GaN, respectively. As shown in Table I, the edge dislocation density of the GaN film grown on 4H-SiC is an order of magnitude lower than that of the GaN film grown on AlN while both films exhibit a relatively comparable screw dislocation density. Previous work indicates that the GaN thermal conductivity is expected to be unaffected by such relatively low screw dislocation densities (on the order of 10^7 cm^{-2}).[37] Moreover, a higher crystalline quality of the GaN film grown on 4H-SiC is evidenced by the narrower E_2(high) Raman linewidth as shown in Fig. 5(c) and Table II. In addition, the residual stress in the films was calculated based on the E_2 (high) mode phonon frequency. GaN on 4H-SiC shows minimal stress, while GaN on AlN exhibits a large tensile stress of ~1 GPa (Table II). The GaN growth process on the AlN substrate did not employ an optimized interlayer which is still

TABLE I. Dislocation densities calculated from XRD rocking curves.

	GaN on SiC	GaN on AlN
Screw dislocation (cm^{-2})	6.14×10^7	2.80×10^7
Edge dislocation (cm^{-2})	3.66×10^8	1.79×10^9

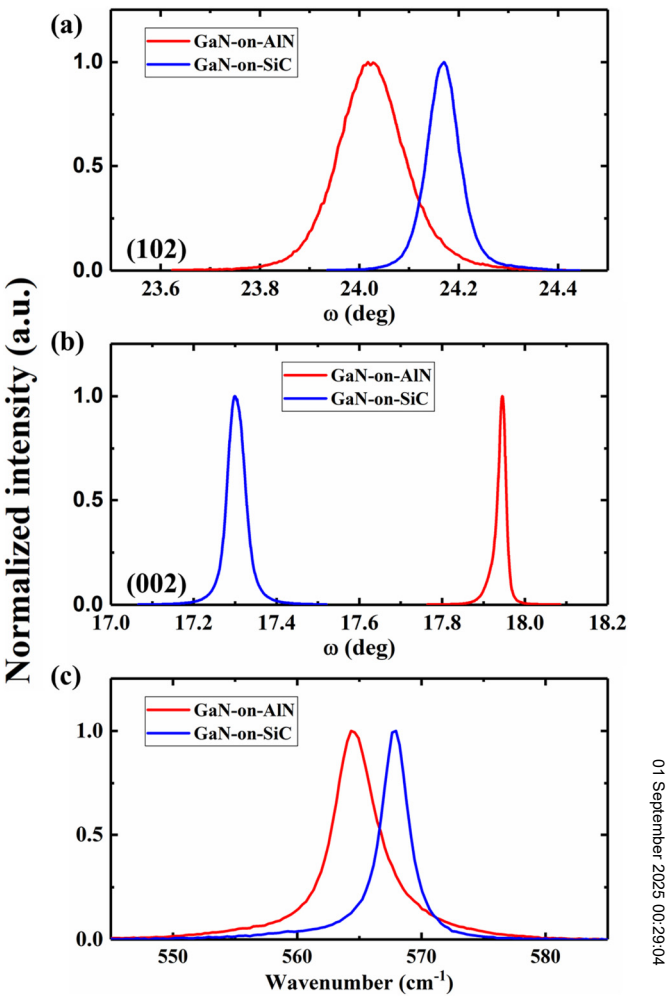

FIG. 5. XRD rocking curves showing (a) the (102) GaN film peaks and (b) the (002) GaN film peaks. (c) Raman spectra of the GaN films showing the E_2 (high) peak. All peaks have been normalized with respect to the maximum intensity.

TABLE II. Raman spectroscopy analysis of the E_2 (high) phonon mode.

	GaN on SiC	GaN on AlN
FWHM (cm^{-1})	2.543 ± 0.013	4.061 ± 0.025
Residual stress (MPa)	48 ± 43	1030 ± 140

required to accommodate the GaN–AlN lattice mismatch of 2.4%. This results in an almost order of magnitude increase in the density of edge-type dislocations in the GaN grown on AlN compared to the GaN film on 4H-SiC (Table I). The inclination of edge-type threading dislocations has been shown to generate a tensile stress gradient in AlGaN[38] and GaN,[39] and a similar mechanism is likely responsible for the tensile stress measured in the GaN film on AlN in this study. XRD and Raman spectroscopy data suggest that the GaN film on 4H-SiC possesses a better crystalline quality, resulting in a higher thermal conductivity as compared to the GaN film grown on AlN. It is likely that lower dislocation density in the GaN would have been obtained if a low temperature GaN or AlGaN buffer layer had been employed and optimized for growth on the AlN substrate.

Figure 4 shows that both GaN films exhibit similar anisotropic thermal transport, with an anisotropic ratio of 1.25–1.3. This indicates that dislocations impact both through-plane and in-plane directions to a similar degree. Therefore, the observed anisotropy can be attributed primarily to phonon-boundary scattering in the through-plane direction, given that the anisotropy is relatively small in a GaN bulk crystal.[36] Additionally, considering that both GaN films have an identical thickness, the XRD and thermal conductivity data reveal that increasing the edge dislocation density by an order of magnitude results in a 40%–50% drop in the GaN thermal conductivity. Moreover, the κ_{out} of the GaN film grown on AlN under elevated temperatures is lower than previously reported values for a 1 μm GaN film grown on SiC,[23] which further confirms the relatively low crystalline quality of this GaN film.

On the contrary, the thermal conductivity of the GaN layer grown on 4H-SiC surpasses values previously reported in the literature as shown in Fig. 4. The measured κ_{out} is comparable to that of a homoepitaxially grown 1.9 μm thick GaN film.[40] In addition, the measured κ_{in} (which is less affected by phonon-boundary scattering) approaches the thermal conductivity of bulk pure GaN calculated by Lindsay *et al.*[36] To confirm the experimental observations (i.e., the bulk-like κ_{in}), κ_{in} was measured using modulation frequencies of 3, 5, and 7 MHz and no frequency-dependent (i.e., depth-dependent) variations were observed in the measurement results. It should be noted that, for high quality MOCVD-grown AlN thin films, a similar observation (i.e., high κ_{in}) was reported by Bin Hoque *et al.*,[41] Koh *et al.*,[42] and Cheng *et al.*[43]

The κ_{out} and κ_{in} of the AlN substrate are plotted in Fig. 6. The measured values and the observed small anisotropy ratio (<0.05 at room temperature) agree with data reported in the literature.[43] The measured thermal conductivities are comparable to the highest values measured[43] and calculated ($\kappa_{out} = 300$ W m^{-1} K^{-1}, $\kappa_{in} = 322$ W m^{-1} K^{-1})[44] for bulk AlN, suggesting the high crystalline quality of the commercial AlN substrate.

The κ_{out} and κ_{in} of the 965 nm thick AlN film grown on 4H-SiC are also plotted in Fig. 6. The measured κ_{out} at room temperature is 198 W m^{-1} K^{-1}. This value slightly exceeds a previously measured κ_{out} for a homoepitaxially grown 1 μm thick AlN film.[15] Figure 6 (dotted line) shows that the temperature-dependent κ_{out} agrees with theoretical predictions for a 1 μm thick AlN film free of Al vacancies.[45] Previous studies calculated that 70% of the AlN bulk thermal conductivity is contributed by phonons with a mean free path (MFP) less than 1 μm,[45] indicating that the κ_{out} of the 965 nm thick AlN layer is limited by phonon-boundary scattering in the out-of-plane (i.e., c-axis) direction. The relatively high κ_{out} for the given thickness[46] suggests that phonon scattering at the starting region of the nucleation layer is insignificant.[41,42] On the other hand, the measured κ_{in} (~253 Wm^{-1}K^{-1}) is comparable to a value reported for a 3 μm thick AlN film with a dislocation density of 1.6×10^8 cm^{-2}, grown by a similar MOCVD method.[41]

The thermal boundary conductance (*TBC*) at the GaN/SiC, GaN/AlN, and AlN/SiC interfaces of the three epitaxial wafers is summarized in Fig. 7 as a function of temperature. Notably, the GaN/SiC *TBC* is found to be higher than a previously reported *TBC* value for GaN/SiC (i.e., GaN directly grown on 4H-SiC)[16] and GaN/SiC with a 36 nm AlN interlayer.[10] The enhancement in the GaN/SiC *TBC* is attributed to the thin (<20 nm) AlN interlayer that bridges the vibrational spectra at the interface, which improves interfacial thermal transport between GaN and SiC.[18] The observed increase in the *TBC* with temperature is primarily due to the increase in the heat capacity (for a temperature range that is below the Debye temperatures of GaN and SiC).[18] In addition, at higher temperatures, inelastic phonon scattering and the higher population of excited phonon modes contribute to the enhancement in the thermal transport across the interface.[18,47]

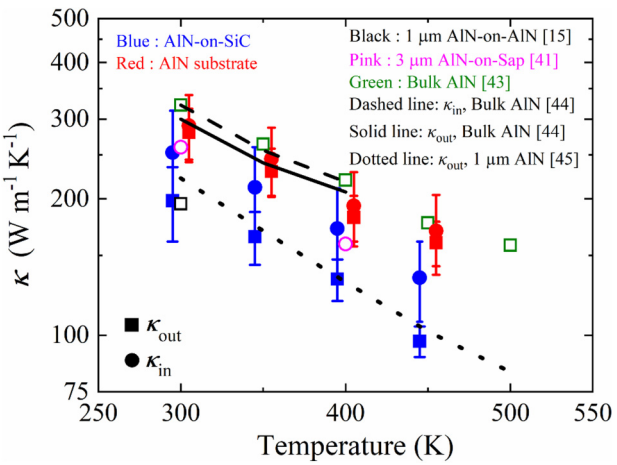

FIG. 6. The measured κ_{out} (squares) and κ_{in} (circles) of the 965 nm thick AlN film on 4H-SiC (blue) and the bulk AlN substrate (red). Open symbols are literature values. The calculated κ_{in} (dashed line) and κ_{out} (solid line) of bulk pure AlN by Lindsay *et al.*[44] are also shown. The dotted line represents the calculated κ_{out} for a pure 1 μm thick AlN film by Xu *et al.*[45] For better visibility, the blue and red data points were, respectively, shifted to the left and right by 5 K.

The room temperature *TBC* at the AlN/SiC interface was found to be 470 MW m^{-2} K^{-1}. At room temperature, the *TBC* at the GaN/AlN interface was determined to be 490 MW m^{-2} K^{-1}. This value is lower than a previously measured GaN/AlN *TBC* (620 MW m^{-2} K^{-1}) for a GaN–AlN superlattice,[48] which might be attributed to the higher dislocation density of the film. Nevertheless, *TBC*s for the GaN/AlN and AlN/SiC interfaces are more than 1.5× higher than those for the GaN/SiC interfaces characterized in this work and in the literature, as shown in Fig. 7. This is attributed to the structural similarity, smaller lattice mismatch, and the closely matched phonon density of states between GaN and AlN as well as AlN and SiC.[49,50]

The measured *TBC* at the AlN/SiC interface increases with temperature. However, the *TBC* at the GaN/AlN interface decreases with temperature, which contradicts the predicted behavior for GaN/AlN interfaces.[49,51–53] This discrepancy may be attributed to a high defect density near the GaN/AlN interface (it should be noted that the GaN-on-AlN wafer tested in this work exhibits a high dislocation density in the GaN layer). A similar observation has been reported for GaN/(AlN)/SiC interfaces with high interfacial defect density (Fig. 7).[22]

To further verify the observed reduction in the GaN/AlN *TBC* with temperature, acoustic echoes[54,55] reflected by the GaN/AlN and GaN/SiC interfaces were monitored via the TDTR signals, as shown in Fig. 8. At room temperature, the amplitude of the acoustic echo reflected by the GaN/AlN interface is lower than that reflected by the GaN/SiC interface. This indicates stronger phonon transmission (i.e., higher *TBC*) through the GaN/SiC interface. Under elevated temperature conditions, the amplitude of the acoustic echo reflected by the GaN/AlN interface increases [Fig. 8(a)] while the amplitude of the acoustic echo reflected by the GaN/SiC interface decreases [Fig. 8(b)] as compared to the room temperature amplitudes. These observations show a qualitative agreement

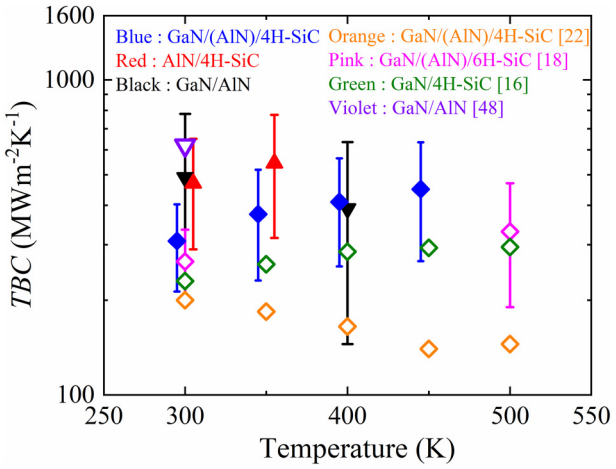

FIG. 7. The measured *TBC* at the GaN/SiC, GaN/AlN, and AlN/SiC interfaces. Open symbols are literature values for different interfaces as labeled (the parentheses indicate the presence of a thin interlayer). For better visibility, the blue and red data points were, respectively, shifted to the left and right by 5 K.

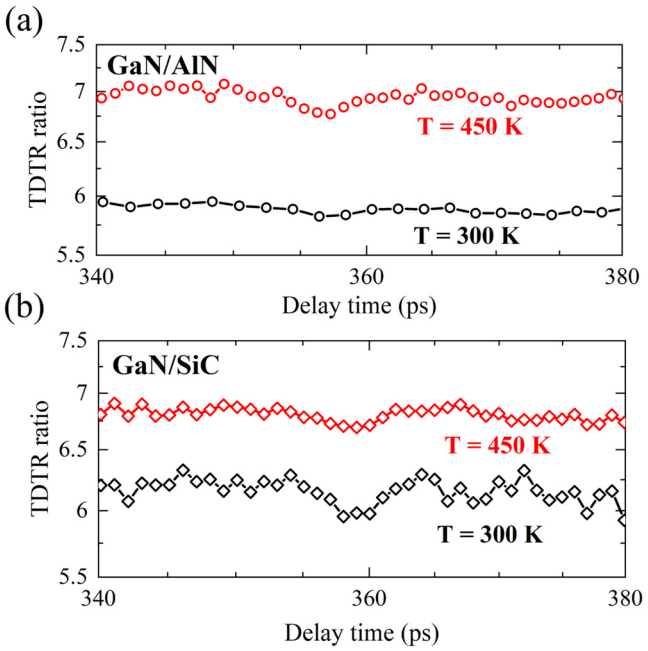

FIG. 8. Portions of the TDTR ratio signals that display the detected acoustic echoes originating from the reflection of the acoustic waves by the (a) GaN/AlN and (b) GaN/SiC interfaces at 300 and 450 K. An offset has been applied to the y-axes for better visibility.

with the observed temperature dependence of the *TBC*s for both interfaces.

It should be noted that some *TBC* values for the GaN/AlN and AlN/SiC interfaces could not be determined under high temperature conditions due to the reduced sensitivity of the TDTR signal, as shown in Figs. 2(c) and 2(d). This is because at high temperatures, the thermal resistance of the GaN and/or AlN epitaxial layers comprises a large portion of the thermal resistance of the material stack due to the decrease in their thermal conductivities while the *TBC* values either increase (in the case of AlN/SiC) or remain at a relatively high value (in the case of GaN/AlN). This also elucidates why the measured *TBC* values at elevated temperatures are accompanied by high uncertainty levels.

VI. CONCLUSION

In summary, thermophysical properties associated with GaN-on-SiC, GaN-on-AlN, and AlN-on-SiC epitaxial wafers were characterized using a multi-frequency/spot-size time-domain thermoreflectance (TDTR) approach. Anisotropic thermal conductivities of the GaN and AlN epitaxial layers as well as the 4H-SiC and AlN substrates were determined. The thermal boundary conductance (*TBC*) between the epitaxial layers and substrates was evaluated over a range of temperatures that are relevant to device operation. The results show that the thermal conductivity of a GaN film directly grown on an AlN substrate with a relatively low crystalline quality is 40%–50% lower than that of a high quality GaN

film (grown on 4H-SiC using a thin AlN interlayer to achieve a high quality GaN layer). The *TBC* at the epitaxial layer/substrate interface of a GaN-on-AlN epitaxial wafer is higher than that of a GaN-on-SiC epitaxial wafer at room temperature. Both wafers exhibit a similar *TBC* value under elevated temperature conditions. The room temperature thermal conductivity (in both c-axis and c-plane directions) of the epitaxial film of an AlN-on-SiC epitaxial wafer is higher than those for the GaN layers grown on 4H-SiC and AlN. The thermophysical property data generated from this work will offer valuable insights into the phonon transport within wide-bandgap semiconductor material stacks/heterostructures and pave the way for the electro-thermal co-design of next generation AlN-incorporated GaN HEMT devices.

DATA AVAILABILITY

The data that support the findings of this study are available from the corresponding author upon reasonable request.

ACKNOWLEDGMENTS

This work was partly supported by the Army Research Office (Department of Army Ultra-Wide Bandgap RF Electronics Center) under Award No. W911NF2220191. This material is partly based upon work supported by the National Science Foundation under Grant No. DMR-2234479 (NSF Future of Semiconductors Teaming Grant). Any opinions, findings, and conclusions or recommendations expressed in this material are those of the authors and do not necessarily reflect the views of the National Science Foundation. T.M. and J.M.R. acknowledge the support from the Air Force Office of Scientific Research (AFOSR) under Award No. FA9550-19-1-0349.

AUTHOR DECLARATIONS

Conflict of Interest

The authors have no conflicts to disclose.

Author Contributions

Husam Walwil: Data curation (lead); Formal analysis (lead); Investigation (lead); Methodology (lead); Visualization (lead); Writing – original draft (lead); Writing – review & editing (lead). **Yiwen Song:** Data curation (supporting); Formal analysis (supporting); Investigation (supporting); Methodology (supporting); Validation (supporting); Visualization (supporting). **Daniel C. Shoemaker:** Investigation (supporting); Writing – original draft (supporting). **Kyuhwe Kang:** Data curation (supporting); Formal analysis (supporting). **Timothy Mirabito:** Formal analysis (supporting). **Joan M. Redwing:** Formal analysis (supporting); Investigation (supporting); Methodology (supporting); Supervision (supporting); Validation (supporting); Writing – original draft (supporting). **Sukwon Choi:** Conceptualization (lead); Formal analysis (supporting); Funding acquisition (lead); Investigation (supporting); Methodology (supporting); Project administration (lead); Resources (lead); Supervision (lead); Validation (supporting); Visualization (supporting); Writing – original draft (supporting); Writing – review & editing (supporting).

DATA AVAILABILITY

The data that support the findings of this study are available from the corresponding author upon reasonable request.

REFERENCES

[1]R. J. Trew, G. L. Bilbro, W. Kuang, Y. Liu, and H. Yin, "Microwave AlGaN/GaN HFETs," IEEE Microwave Mag. **6**, 56–66 (2005).
[2]R. Ma, K. H. Teo, S. Shinjo, K. Yamanaka, and P. M. Asbeck, "A GaN PA for 4G LTE-advanced and 5G: Meeting the telecommunication needs of various vertical sectors including automobiles, robotics, health care, factory automation, agriculture, education, and more," IEEE Microwave Mag. **18**(7), 77–85 (2017).
[3]T. Kaneko, K. Shiikuma, and K. Kunihiro, "GaN HEMT high efficiency power amplifiers for 4G/5G mobile communication base stations," in *2014 Asia-Pacific Microwave Conference* (IEEE, 2014), pp. 994–997.
[4]K. Yuk, G. R. Branner, and C. Cui, "Future directions for GaN in 5G and satellite communications," in *2017 IEEE 60th International Midwest Symposium on Circuits and Systems (MWSCAS)* (IEEE, 2017), pp. 803–806.
[5]S. Ganguly, K. M. Bothe, A. Niyonzima, T. Smith, Y. Liu, J. Fisher, F. Radulescu, D. A. Gajewski, S. T. Sheppard, J. W. Milligan, B. Noori, and J. W. Palmour, "DC and RF reliability assessment of 5G-MMW capable GaN HEMT process (invited)," in *2022 IEEE International Reliability Physics Symposium (IRPS)* (IEEE, 2022), pp. 11B.5-1–11B.5-6.
[6]A. Bar-Cohen, J. J. Maurer, and D. H. Altman, "Embedded cooling for wide bandgap power amplifiers: A review," J. Electron. Packag. **141**(4), 040803 (2019).
[7]X. Qian, P. Jiang, and R. Yang, "Anisotropic thermal conductivity of 4H and 6H silicon carbide measured using time-domain thermoreflectance," Mater. Today Phys. **3**, 70–75 (2017).
[8]E. Cho, A. Mogilatenko, F. Brunner, E. Richter, and M. Weyers, "Impact of AlN nucleation layer on strain in GaN grown on 4H-SiC substrates," J. Cryst. Growth **371**, 45–49 (2013).
[9]R. S. Pengelly, S. M. Wood, J. W. Milligan, S. T. Sheppard, and W. L. Pribble, "A review of GaN on SiC high electron-mobility power transistors and MMICs," IEEE Trans. Microwave Theory Tech. **60**(6 PART 2), 1764–1783 (2012).
[10]J. Cho, Y. Li, D. H. Altman, W. E. Hoke, M. Asheghi, and K. E. Goodson, "Temperature dependent thermal resistances at GaN-substrate interfaces in GaN composite substrates," in *Tech Dig—IEEE Compound Semiconductor Integrated Circuit Symposium (CSIC)* (IEEE, 2012), pp. 5–8.
[11]M. Qi, G. Li, S. Ganguly, P. Zhao, X. Yan, J. Verma, and D. Jena, "Strained GaN quantum-well FETs on single crystal bulk AlN substrates," Appl. Phys. Lett. **110**(6), 63501 (2017).
[12]A. Hickman, R. Chaudhuri, S. J. Bader, K. Nomoto, K. Lee, H. G. Xing, and D. Jena, "High breakdown voltage in RF AlN/GaN/AlN quantum well HEMTs," IEEE Electron Device Lett. **40**(8), 1293–1296 (2019).
[13]J. Kotani, J. Yaita, K. Homma, S. Ozaki, A. Yamada, M. Sato, T. Ohki, and N. Nakamura, "24.4 w/mm X-band GaN HEMTs on AlN substrates with the LPCVD-grown high-breakdown-field SiNxLayer," IEEE J. Electron Devices Soc. **11**(2022), 101–106 (2023).
[14]R. Chaudhuri, *Integrated Electronics on Aluminum Nitride* (Springer Theses) (Springer International Publishing, 2022), pp. 239–246.
[15]G. Alvarez-Escalante, R. Page, R. Hu, H. G. Xing, D. Jena, and Z. Tian, "High thermal conductivity and ultrahigh thermal boundary conductance of homoepitaxial AlN thin films," APL Mater. **10**(1), 011115 (2022).
[16]E. Ziade, J. Yang, G. Brummer, D. Nothern, T. Moustakas, and A. J. Schmidt, "Thermal transport through GaN-SiC interfaces from 300 to 600 K," Appl. Phys. Lett. **107**(9), 091605 (2015).
[17]F. Mu, Z. Cheng, J. Shi, S. Shin, B. Xu, J. Shiomi, S. Graham, and T. Suga, "High thermal boundary conductance across bonded heterogeneous GaN-SiC interfaces," ACS Appl. Mater. Interfaces **11**(36), 33428–33434 (2019).
[18]R. Li, K. Hussain, M. E. Liao, K. Huynh, M. S. B. Hoque, S. Wyant, Y. R. Koh, Z. Xu, Y. Wang, D. P. Luccioni, Z. Cheng, J. Shi, E. Lee, S. Graham, A. Henry, P. E. Hopkins, M. S. Goorsky, M. A. Khan, and T. Luo, "Enhanced thermal

boundary conductance across GaN/SiC interfaces with AlN transition layers," ACS Appl. Mater. Interfaces **16**(6), 8109–8118 (2024).
[19]D. G. Cahill, W. K. Ford, K. E. Goodson, G. D. Mahan, A. Majumdar, H. J. Maris, and S. R. Phillpot, "Nanoscale thermal transport," J. Appl. Phys. **93**(2), 793–818 (2003).
[20]P. Jiang, X. Qian, and R. Yang, "Tutorial: Time-domain thermoreflectance (TDTR) for thermal property characterization of bulk and thin film materials," J. Appl. Phys. **124**(16), 161103 (2018).
[21]Y. Song, C. Perez, G. Esteves, J. S. Lundh, C. B. Saltonstall, T. E. Beechem, and S. Choi, "Thermal conductivity of aluminum scandium nitride for 5G mobile applications and beyond," ACS Appl. Mater. Interfaces **13**(16), 19031–19041 (2021).
[22]J. Cho, Y. Li, W. E. Hoke, D. H. Altman, M. Asheghi, and K. E. Goodson, "Phonon scattering in strained transition layers for GaN heteroepitaxy," Phys. Rev. B **89**(11), 115301 (2014).
[23]E. Ziade, J. Yang, G. Brummer, D. Nothern, T. Moustakas, and A. J. Schmidt, "Thickness dependent thermal conductivity of gallium nitride," Appl. Phys. Lett. **110**(3), 031903 (2017).
[24]C. Wei, X. Zheng, D. G. Cahill, and J. C. Zhao, "Invited article: Micron resolution spatially resolved measurement of heat capacity using dual-frequency time-domain thermoreflectance," Rev. Sci. Instrum. **84**(7), 071301 (2013).
[25]P. Jiang, X. Qian, and R. Yang, "Time-domain thermoreflectance (TDTR) measurements of anisotropic thermal conductivity using a variable spot size approach," Rev. Sci. Instrum. **88**(7), 074901 (2017).
[26]Y. K. Koh and D. G. Cahill, "Frequency dependence of the thermal conductivity of semiconductor alloys," Phys. Rev. B **76**(7), 075207 (2007).
[27]A. J. Minnich, J. A. Johnson, A. J. Schmidt, K. Esfarjani, M. S. Dresselhaus, K. A. Nelson, and G. Chen, "Thermal conductivity spectroscopy technique to measure phonon mean free paths," Phys. Rev. Lett. **107**(9), 1–4 (2011).
[28]D. G. Cahill, "Analysis of heat flow in layered structures for time-domain thermoreflectance," Rev. Sci. Instrum. **75**(12), 5119–5122 (2004).
[29]Y. K. Koh, S. L. Singer, W. Kim, J. M. O. Zide, H. Lu, D. G. Cahill, A. Majumdar, and A. C. Gossard, "Comparison of the 3ω method and time-domain thermoreflectance for measurements of the cross-plane thermal conductivity of epitaxial semiconductors," J. Appl. Phys. **105**(5), 054303 (2009).
[30]Q. Zheng, C. Li, A. Rai, J. H. Leach, D. A. Broido, and D. G. Cahill, "Thermal conductivity of GaN, GaN 71, and SiC from 150 K to 850 K," Phys. Rev. Mater. **3**(1), 014601 (2019).
[31]H. Li, R. Hanus, C. A. Polanco, A. Zeidler, G. Koblmüller, Y. K. Koh, and L. Lindsay, "Gan thermal transport limited by the interplay of dislocations and size effects," Phys. Rev. B **102**(1), 014313 (2020).
[32]B. Sun, G. Haunschild, C. Polanco, J. Ju, L. Lindsay, G. Koblmüller, and Y. K. Koh, "Dislocation-induced thermal transport anisotropy in single-crystal group-III nitride films," Nat. Mater. **18**(2), 136–140 (2019).
[33]T. Metzger, R. Höpler, E. Born, O. Ambacher, M. Stutzmann, R. Stömmer, and H. P. Strunk, "Defect structure of epitaxial GaN films determined by transmission electron microscopy and triple-axis x-ray diffractometry," Philos. Mag. A **77**(4), 1013–1025 (1998).
[34]R. Chierchia, T. Böttcher, H. Heinke, S. Einfeldt, S. Figge, and D. Hommel, "Microstructure of heteroepitaxial GaN revealed by x-ray diffraction," J. Appl. Phys. **93**(11), 8918–8925 (2003).
[35]S. Choi, E. Heller, D. Dorsey, R. Vetury, and S. Graham, "Analysis of the residual stress distribution in AlGaN/GaN high electron mobility transistors," J. Appl. Phys. **113**(9), 093510 (2013).
[36]L. Lindsay, D. A. Broido, and T. L. Reinecke, "Thermal conductivity and large isotope effect in GaN from first principles," Phys. Rev. Lett. **109**(9), 095901 (2012).
[37]K. Termentzidis, M. Isaiev, A. Salnikova, I. Belabbas, D. Lacroix, and J. Kioseoglou, "Impact of screw and edge dislocations on the thermal conductivity of individual nanowires and bulk GaN: A molecular dynamics study," Phys. Chem. Chem. Phys. **20**(7), 5159–5172 (2018).
[38]A. E. Romanov, G. E. Beltz, P. Cantu, F. Wu, S. Keller, S. P. DenBaars, and J. S. Speck, "Cracking of III-nitride layers with strain gradients," Appl. Phys. Lett. **89**(16), 161922 (2006).
[39]S. Raghavan, I. C. Manning, X. Weng, and J. M. Redwing, "Dislocation bending and tensile stress generation in GaN and AlGaN films," J. Cryst. Growth **359**, 35–42 (2012).
[40]Y. R. Koh, M. S. Bin Hoque, H. Ahmad, D. H. Olson, Z. Liu, J. Shi, and P. E. Hopkins, "High thermal conductivity and thermal boundary conductance of homoepitaxially grown gallium nitride (GaN) thin films," Phys. Rev. Mater. **5**(10), 104604 (2021).
[41]M. S. Bin Hoque, Y. R. Koh, J. L. Braun, A. Mamun, Z. Liu, K. Huynh, M. E. Liao, K. Hussain, Z. Cheng, E. R. Hoglund, D. H. Olson, J. A. Tomko, K. Aryana, R. Galib, J. T. Gaskins, M. M. M. Elahi, Z. C. Leseman, J. M. Howe, T. Luo, S. Graham, M. S. Goorsky, A. Khan, and P. E. Hopkins, "High in-plane thermal conductivity of aluminum nitride thin films," ACS Nano **15**(6), 9588–9599 (2021).
[42]Y. R. Koh, Z. Cheng, A. Mamun, M. S. Bin Hoque, Z. Liu, T. Bai, K. Hussain, M. E. Liao, R. Li, J. T. Gaskins, A. Giri, J. Tomko, J. L. Braun, M. Gaevski, E. Lee, L. Yates, M. S. Goorsky, T. Luo, A. Khan, S. Graham, and P. E. Hopkins, "Bulk-like intrinsic phonon thermal conductivity of micrometer-thick AlN films," ACS Appl. Mater. Interfaces **12**(26), 29443–29450 (2020).
[43]Z. Cheng, Y. R. Koh, A. Mamun, J. Shi, T. Bai, K. Huynh, L. Yates, Z. Liu, R. Li, E. Lee, M. E. Liao, Y. Wang, H. M. Yu, M. Kushimoto, T. Luo, M. S. Goorsky, P. E. Hopkins, H. Amano, A. Khan, and S. Graham, "Experimental observation of high intrinsic thermal conductivity of AlN," Phys. Rev. Mater. **4**(4), 44602 (2020).
[44]L. Lindsay, D. A. Broido, and T. L. Reinecke, "*Ab initio* thermal transport in compound semiconductors," Phys. Rev. B **87**(16), 165201 (2013).
[45]R. L. Xu, M. Munõz Rojo, S. M. Islam, A. Sood, B. Vareskic, A. Katre, N. Mingo, K. E. Goodson, H. G. Xing, D. Jena, and E. Pop, "Thermal conductivity of crystalline AlN and the influence of atomic-scale defects," J. Appl. Phys. **126**(18), 185105 (2019).
[46]Y. Song, C. Zhang, J. S. Lundh, H.-L. Huang, Y. Zheng, Y. Zhang, M. Park, T. Mirabito, R. Beaucejour, C. Chae, N. McIlwaine, G. Esteves, T. E. Beechem, C. Moe, R. Dargis, J. Jones, J. H. Leach, R. M. Lavelle, D. W. Snyder, J.-P. Maria, R. H. Olsson, J. M. Redwing, A. Ansari, J. Hwang, X. Wang, B. M. Foley, S. E. Trolier-McKinstry, and S. Choi, "Growth-microstructure-thermal property relations in AlN thin films," J. Appl. Phys. **132**(17), 175108 (2022).
[47]E. S. Landry and A. J. H. McGaughey, "Thermal boundary resistance predictions from molecular dynamics simulations and theoretical calculations," Phys. Rev. B **80**(16), 165304 (2009).
[48]Y. K. Koh, Y. Cao, D. G. Cahill, and D. Jena, "Heat-transport mechanisms in superlattices," Adv. Funct. Mater. **19**(4), 610–615 (2009).
[49]Q. Wang, X. Wang, X. Liu, and J. Zhang, "Interfacial engineering for the enhancement of interfacial thermal conductance in GaN/AlN heterostructure," J. Appl. Phys. **129**(23), 235102 (2021).
[50]X. Li and R. Yang, "Effect of lattice mismatch on phonon transmission and interface thermal conductance across dissimilar material interfaces," Phys. Rev. B **86**, 054305 (2012).
[51]J. Sun, Y. Li, Y. Karaaslan, C. Sevik, and Y. Chen, "Misfit dislocation structure and thermal boundary conductance of GaN/AlN interfaces," J. Appl. Phys. **130**, 035301 (2021).
[52]C. A. Polanco and L. Lindsay, "Phonon thermal conductance across GaN-AlN interfaces from first principles," Phys. Rev. B **99**(7), 075202 (2019).
[53]T. Feng, H. Zhou, Z. Cheng, L. S. Larkin, and M. R. Neupane, "A critical review of thermal boundary conductance across wide and ultrawide bandgap semiconductor interfaces," ACS Appl. Mater. Interfaces **15**, 29655–29673 (2023).
[54]K. E. O'Hara, X. Hu, and D. G. Cahill, "Characterization of nanostructured metal films by picosecond acoustics and interferometry," J. Appl. Phys. **90**, 4852–4858 (2001).
[55]Z. Cheng, F. Mu, X. Ji, T. You, W. Xu, T. Suga, X. Ou, D. G. Cahill, and S. Graham, "Thermal visualization of buried interfaces enabled by ratio signal and steady-state heating of time-domain thermoreflectance," ACS Appl. Mater. Interfaces **13**, 31843–31851 (2021).